

Generation of single entangled photon-phonon pairs via an atom-photon-phonon interaction

Xun-Wei Xu,^{1,*} Hai-Quan Shi,^{2,1} Jie-Qiao Liao,³ and Ai-Xi Chen^{4,1,†}

¹*Department of Applied Physics, East China Jiaotong University, Nanchang, 330013, China*

²*School of Materials Science and Engineering, Nanchang University, Nanchang 330031, China*

³*Key Laboratory of Low-Dimensional Quantum Structures and Quantum Control of Ministry of Education, Department of Physics and Synergetic Innovation Center for Quantum Effects and Applications, Hunan Normal University, Changsha 410081, China*

⁴*Department of Physics, Zhejiang Sci-Tech University, Hangzhou 310018, China*

(Dated: May 8, 2019)

Quantum blockade and entanglement play important roles in quantum information and quantum communication as quantum blockade is an effective mechanism to generate single photons (phonons) and entanglement is a crucial resource for quantum information processing. In this work, we propose a method to generate single entangled photon-phonon pairs in a hybrid optomechanical system. We show that photon blockade, phonon blockade, and photon-phonon correlation and entanglement can be observed via the atom-photon-phonon (tripartite) interaction, under the resonant atomic driving. The correlated and entangled single photons and single phonons, i.e., single entangled photon-phonon pairs, can be generated in both the weak and strong tripartite interaction regimes. Our results may have important applications in the development of highly complex quantum networks.

I. INTRODUCTION

Optomechanical systems with parametric coupling between optical and mechanical modes provide us a perfect platform for manipulating the states of photons and phonons [1]. As an important application, photon (phonon) blockade [2–4], that only allows single photon (phonon) excitation in the optical (mechanical) mode, based on optomechanical interaction has attracted significant interest in the past few years. A number of designs based on diverse mechanisms are proposed to demonstrate photon (phonon) blockade in optomechanical systems, such as photon (phonon) blockade based on strong optomechanical couplings [5–15] and photon (phonon) blockade in weak nonlinear regime induced by quantum interference [16–20].

In a recent experiment [21], the non-classical correlations between single photons and phonons from a nanomechanical resonator was reported by driving the nanomechanical photonic crystal cavity with blue-detuned optical pulse. After that, we studied the photon and phonon statistics in a quadratically coupled optomechanical system, and show that both photon blockade and phonon blockade can be observed in the same parameter regime, and more important, the single photons and single phonons are strongly anticorrelated [22]. Here, we will do a further study and propose a method to generate correlated single photons and single phonons under the constant atomic driving. Even more interestingly, we will show that the correlated single photons and single phonons are entangled with each other, i.e., they are single entangled photon-phonon pairs.

Entangled states have great significance of both fundamental physics study and applications in quantum information processing and quantum communication. The optomechanical entanglement has already been proposed theoretically [23–28] and demonstrated experimentally [29–32]. Optomechanical systems provide a perfect platform to generate both bipartite [33–36] and multipartite [37–41] entanglement. However, there are substantial differences between the entanglement we will discuss in this paper and entanglement proposed before. One striking difference is the entanglement we proposed here is for single photons and phonons, which is non-Gaussian, so that the generally adopted method, i.e., the linearization of the optomechanical interaction, is no longer applicable.

Inspired by a recent experiment [42], in which the coupling between an optomechanical resonator with two-level emitters was realized, here we consider a hybrid system which enables a tripartite interaction between a two-level atom, an optical mode, and a mechanical mode [43]. We study the generation of single entangled photon-phonon pairs, which are useful for quantum information and quantum communication. Such atom-photon-phonon interactions were proposed to provide an optically controllable interaction between a two-level atom and a macroscopic mechanical oscillator [19, 44] by driving the optical mode strongly. Nevertheless, in this paper we drive the two-level atom coherently and show that single entangled photon-phonon pairs can be generated in the hybrid optomechanical system. The single entangled photon-phonon pairs have potential application in the development of highly complex quantum networks.

The remainder of this paper is organized as follows. In Sec. II, we introduce the theoretical model of a hybrid optomechanical system, and show the simple derivation of the atom-photon-phonon interaction and the energy spectrum of the Hamiltonian. In Sec. III, the photon and

* davidxu0816@163.com

† aixichen@zstu.edu.cn

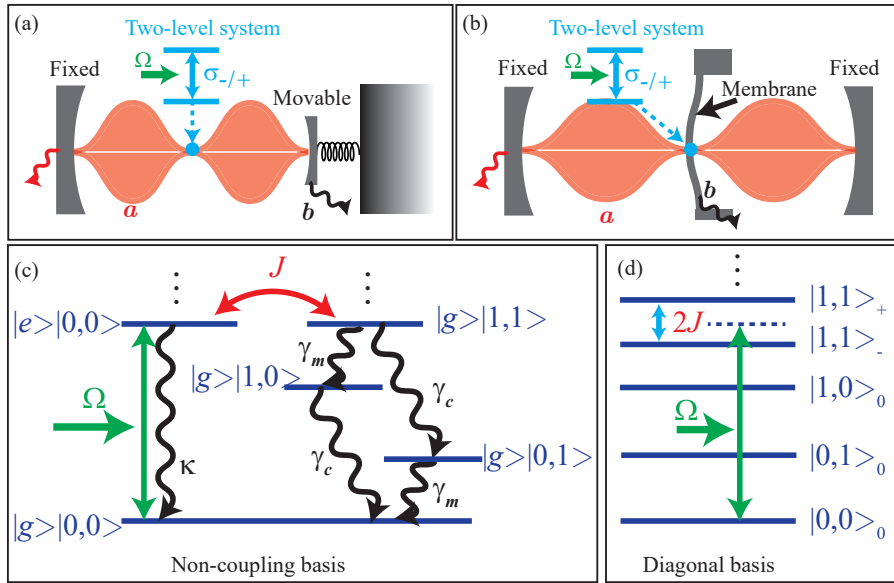


FIG. 1. (Color online) Schematics of the hybrid systems with atom-photon-phonon interactions: (a) a two-level atom in an optical cavity with a movable end mirror: (b) a two-level atom imbedded in a membrane inside an optical cavity. The energy spectrum of the hybrid optomechanical system [see the Hamiltonian in Eq. (5)] given (c) in the non-coupling basis and (d) in the diagonal basis.

phonon statistics, and the quantum correlation between the photons and phonons are discussed numerically. Finally, a summary is given in Sec. IV.

II. MODEL AND HAMILTONIAN

We study a hybrid system with a two-level atom (σ_{\pm} being the ladder operators) of transition frequency ω_0 and a mechanical resonator b of resonance frequency ω_m in an optical cavity a of resonance frequency ω_c , as shown in Fig. 1(a) and (b). Here, we consider a special situation

in which the mechanical displacement x induces a variation of the spatial distribution of the cavity field [44], while the mechanical effect on the optical frequency ω_c can be neglected. Thus, the coupling strength $g(x)$ between the two-level atom and the optical mode depends on the position of the mechanical resonator x , which is described by the interaction Hamiltonian under the rotating-wave approximation as ($\hbar = 1$)

$$H_{\text{int}} = g(x) (\sigma_+ a + \sigma_- a^\dagger). \quad (1)$$

Typically the mechanical displacement x is very small, and $g(x)$ can be expanded to the first order in x ,

$$g(x) = g(0) + J(b^\dagger + b), \quad (2)$$

where $J \equiv (\partial g / \partial x)|_{x=0} x_{\text{zpf}}$ is the tripartite atom-photon-phonon interaction strength. In the specific condition that the two-level atom is placed at the node of the optical mode with mechanical resonator in equilibrium, i.e., $g(0) = 0$, and the only possible interaction between them is the atom-photon-phonon interaction as

$$H_{\text{int}} = J(b^\dagger + b) (\sigma_+ a + \sigma_- a^\dagger). \quad (3)$$

Under particular resonant conditions, the tripartite interaction allows swapping the excitation between the three quantum systems. Under the conditions $\omega_0 = \omega_c + \omega_m$

and $\min\{\omega_0, \omega_c\} \gg \omega_m \gg J$, the Hamiltonian of the resonant interaction reads

$$H_{\text{int}} = J(\sigma_+ ab + \sigma_- a^\dagger b^\dagger), \quad (4)$$

which describes the simultaneous generation of a photon and a phonon with the two-level atom jumping from the excited state to its ground state and the reverse process. This tripartite interaction provides us an effective way to generate photon-phonon pairs. Such a hybrid system can be implemented in the electromechanical systems [29, 45–47] with artificial atom at the node or in a Fabry-Pérot cavity with a membrane containing two-level atoms in the node of the cavity mode [48–51].

Next, we consider the case that the two-level atom is pumped by a coherent field (strength Ω , frequency ω_p), and the total Hamiltonian for the hybrid sys-

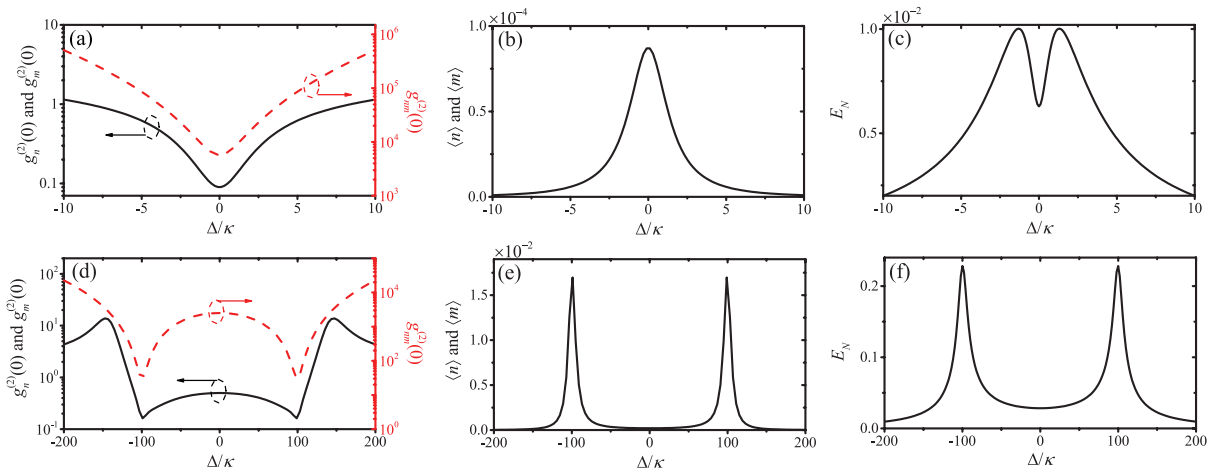


FIG. 2. (Color online) In panels (a) and (d), the equal-time second-order correlation functions [$g_n^{(2)}(0)$ and $g_m^{(2)}(0)$] and cross-correlation function $g_{nm}^{(2)}(0)$ are plotted as functions of the detuning Δ/κ . In panels (b) and (e), the mean photon (phonon) number [$\langle n \rangle = \langle m \rangle$] is plotted as a function of the detuning Δ/κ . In panels (c) and (f), the logarithmic negativity E_N is plotted as a function of the detuning Δ/κ . We set $J = 0.1\kappa$ in (a) and (b) and set $J = 100\kappa$ in (c) and (d). Other used parameters are $\gamma_c = \gamma_m = 10\kappa$, $\Omega = \kappa$, and $m_{\text{th}} = 0$.

tem in the rotating frame with respect to $R(t) = \exp[i\omega_p\sigma_+\sigma_-t + i(\omega_p - \omega_m)a^\dagger at + i\omega_m b^\dagger bt]$ reads

$$H = \Delta\sigma_+\sigma_- + \Delta a^\dagger a + J(\sigma_+ ab + \sigma_- a^\dagger b^\dagger) + \Omega\sigma_x, \quad (5)$$

where we introduce the detuning $\Delta \equiv \omega_0 - \omega_p = \omega_c + \omega_m - \omega_p$.

The energy spectrum of the Hamiltonian in Eq. (5) for hybrid optomechanical system is shown in Figs. 1(c) and 1(d). In the non-coupling basis [Fig. 1(c)], $|e\rangle$ ($|g\rangle$)

denotes the excited (ground) state of the two-level atom, and $|n, m\rangle$ represents the Fock state with n photons in the optical mode and m phonons in the mechanical mode. In Fig. 1(d), we denote the eigenstates in the diagonal basis as $|0, 0\rangle_0 \equiv |g\rangle|0, 0\rangle$, $|1, 0\rangle_0 \equiv |g\rangle|1, 0\rangle$, $|0, 1\rangle_0 \equiv |g\rangle|0, 1\rangle$, $|1, 1\rangle_\pm \equiv (|g\rangle|1, 1\rangle \pm |e\rangle|0, 0\rangle)/\sqrt{2}$ with eigenvalues 0, ω_c , ω_m , $\omega_0 \pm J$, respectively.

III. CORRELATION AND ENTANGLEMENT

To quantify the statistics of the phonons and photons in the system, we consider the equal-time second-order correlation functions $g_n^{(2)}(0)$ and $g_m^{(2)}(0)$, and cross-correlation function $g_{nm}^{(2)}(0)$ in the steady state ($t \rightarrow \infty$) defined by

$$g_n^{(2)}(0) \equiv \frac{\langle a^\dagger a^\dagger a a \rangle}{\langle n \rangle^2}, \quad (6)$$

$$g_m^{(2)}(0) \equiv \frac{\langle b^\dagger b^\dagger b b \rangle}{\langle m \rangle^2}, \quad (7)$$

$$g_{nm}^{(2)}(0) \equiv \frac{\langle a^\dagger b^\dagger b a \rangle}{\langle n \rangle \langle m \rangle}, \quad (8)$$

where $\langle n \rangle \equiv \langle a^\dagger a \rangle$ and $\langle m \rangle \equiv \langle b^\dagger b \rangle$ are the mean photon and phonon numbers. The dynamic behavior of the total open system is described by the master equation for the

density matrix ρ of the system [52]

$$\begin{aligned} \frac{\partial \rho}{\partial t} = & -i[H, \rho] + \kappa L[\sigma_-]\rho + \gamma_c L[a]\rho \\ & + \gamma_m(m_{\text{th}} + 1)L[b]\rho + \gamma_m m_{\text{th}} L[b^\dagger]\rho, \end{aligned} \quad (9)$$

where $L[o]\rho = o\rho o^\dagger - (o^\dagger o\rho + \rho o^\dagger o)/2$ denotes a Lindblad term for an operator o ; κ is the damping rate of the two-level atom and γ_c (γ_m) is the damping rate of the optical (mechanical) mode; m_{th} is the mean thermal phonon number. We assume that the frequencies of the two-level atom and the optical mode are so high that the thermal effect can be neglected.

The equal-time second-order correlation functions [$g_n^{(2)}(0)$ and $g_m^{(2)}(0)$] and cross-correlation function $g_{nm}^{(2)}(0)$ are plotted as functions of the detuning Δ/κ in Fig. 2 under both weak-coupling condition [(a) $J = 0.1\kappa$] and strong-coupling condition [(c) $J = 100\kappa$]. It is clear that photon blockade and phonon blockade, i.e., $g_n^{(2)}(0) = g_m^{(2)}(0) < 1$, appear simultaneously around $|\Delta| = J$ for

the same parameters. Simultaneously, the single photons and single phonons generated by photon blockade and phonon blockade are strongly correlated with each other, i.e., $g_{nm}^{(2)}(0) \gg 1$. The optimal detuning Δ for correlated photon blockade and phonon blockade depends on the coupling strength J : $\Delta = 0$ for weak coupling and $|\Delta| \approx J$ for strong coupling. Moreover, the mean photon (phonon) number $\langle n \rangle = \langle m \rangle$ in the weak-coupling case is much smaller than the one in the strong-coupling case.

Physically, the single photon and phonon pairs are generated one by one with the two-level atom jumping from the excited state to its ground state. In the weak-coupling regime ($J \ll \kappa$), the system is driven resonantly with detuning $\Delta = 0$ because the states $|1, 1\rangle_+$ and $|1, 1\rangle_-$ are not resolved. In the strong-coupling regime ($J \gg \kappa$), the system should be investigated by the dressed states as shown in Fig. 1(d), and the single photon and phonon pairs are generated with detuning $\Delta = \pm J$ for resonant pumping.

In order to understand the behavior of the cross-correlation function $g_{nm}^{(2)}(0)$, we can give the expression of $g_{nm}^{(2)}(0)$ approximately. Under the weak-exciting condition, i.e., $\max\{\langle n \rangle, \langle m \rangle\} \ll 1$, we have mean photon (phonon) number

$$\langle n \rangle \approx \rho_{5,5} + \rho_{4,4}, \quad (10)$$

$$\langle m \rangle \approx \rho_{5,5} + \rho_{3,3}, \quad (11)$$

and the cross-correlation function $g_{nm}^{(2)}(0)$

$$g_{nm}^{(2)}(0) \approx \frac{\rho_{5,5}}{(\rho_{5,5} + \rho_{3,3})(\rho_{5,5} + \rho_{4,4})}, \quad (12)$$

where $\rho_{3,3} = \langle g | \langle 0, 1 | \rho | g \rangle | 0, 1 \rangle$, $\rho_{4,4} = \langle g | \langle 1, 0 | \rho | g \rangle | 1, 0 \rangle$, and $\rho_{5,5} = \langle g | \langle 1, 1 | \rho | g \rangle | 1, 1 \rangle$, and they satisfy the relations

$$\rho_{3,3} \approx \frac{\gamma_c}{\gamma_m} \rho_{5,5}, \quad (13)$$

$$\rho_{4,4} \approx \frac{\gamma_m}{\gamma_c} \rho_{5,5}. \quad (14)$$

If we set $\gamma_c = \gamma_m$, then we have $\rho_{3,3} \approx \rho_{4,4} \approx \rho_{5,5}$, $\langle n \rangle = \langle m \rangle \approx 2\rho_{5,5}$, and

$$g_{nm}^{(2)}(0) \approx \frac{1}{2\langle n \rangle}. \quad (15)$$

Under the resonant conditions at the detuning $|\Delta| = J$, we have maximum $\langle n \rangle = \langle m \rangle$, and thus minimum cross-correlation function $g_{nm}^{(2)}(0)$, corresponding to the dips around the detuning $|\Delta| = J$.

It's not hard to guess that the strongly correlated single photons and single phonons generated by photon blockade and phonon blockade are entangled with each other. The entanglement between the optical and mechanical

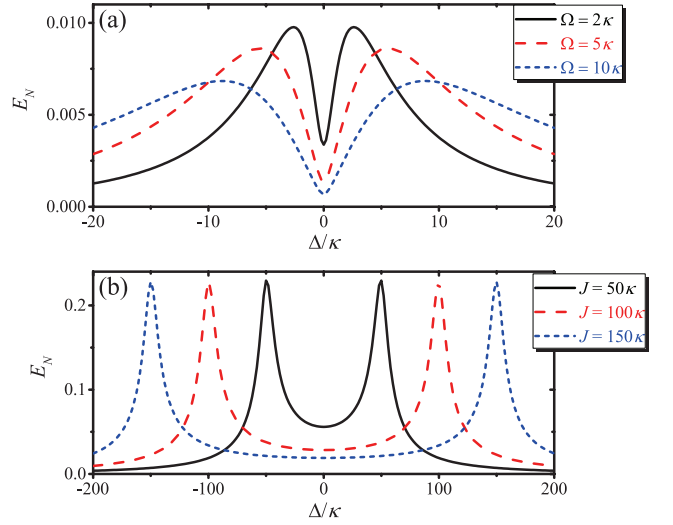


FIG. 3. (Color online) The logarithmic negativity E_N is plotted as a function of the detuning Δ/κ for different driving strength Ω in (a) and for different coupling strength J in (b). We set $J = 0.1\kappa$ in (a) and set $\Omega = \kappa$ in (b). Other used parameters are $\gamma_c = \gamma_m = 10\kappa$ and $m_{\text{th}} = 0$.

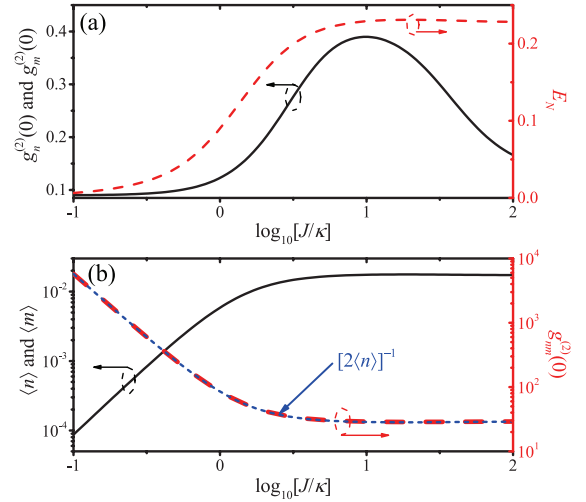


FIG. 4. (Color online) (a) The equal-time second-order correlation functions [$g_n^{(2)}(0)$ and $g_m^{(2)}(0)$] the logarithmic negativity E_N are plotted as functions of the coupling strength $\log_{10}[J/\kappa]$. (b) The mean photon (phonon) number [$\langle n \rangle$ and $\langle m \rangle$] and cross-correlation function $g_{nm}^{(2)}(0)$ are plotted as functions of $\log_{10}[J/\kappa]$. There are two curves for $g_{nm}^{(2)}(0)$, where the red dashed one is obtained from Eq. (9) and the blue short-dashed one is obtained from Eq. (15). Other used parameters are $|\Delta| = J$, $\gamma_c = \gamma_m = 10\kappa$, $\Omega = \kappa$, and $m_{\text{th}} = 0$.

modes can be characterized by the logarithmic negativity [53]

$$E_N = \log_2 \left\| \rho_{AB}^{TA} \right\|_1, \quad (16)$$

where the symbol $\|\cdot\|_1$ denotes the trace norm, and ρ_{AB}^{TA}

is the partial transpose of the reduced density matrix ρ_{AB} of the optical and mechanical modes. It is worth mentioning that the entangled state for the single photons and single phonons obtained here is non-Gaussian. Thus the logarithmic negativity for Gaussian states [59] widely used in the previous works [23–28] cannot be used to accurately describe the entangled state here.

The logarithmic negativity E_N is shown in Figs. 2(c) and 2(f). Obviously, the strongly correlated single photons and single phonons generated by photon blockade and phonon blockade are entangled with each other in both the weak ($J < \kappa$) and strong ($J > \kappa$) coupling regimes. In the weak-coupling regime as shown in Fig. 2(c), there is a dip around the detuning $\Delta = 0$, which is induced by the quantum interferences between two routes: (a) the direct transition channel $|g\rangle|0,0\rangle \xrightarrow{\Omega} |e\rangle|0,0\rangle \xrightarrow{J} |g\rangle|1,1\rangle$; (b) the indirect transition channel $|g\rangle|0,0\rangle \xrightarrow{\Omega} |e\rangle|0,0\rangle \xrightarrow{\Omega} |g\rangle|0,0\rangle \xrightarrow{\Omega} |e\rangle|0,0\rangle \xrightarrow{J} |g\rangle|1,1\rangle$ (or higher-order variants). Thus the width of the dip depends on the driving strength Ω , as shown in Fig. 3(a). Similar mechanism can induce transparency in lambda-type three-level atoms [54, 55] and optomechanical systems [56–58]. Differently, in Fig. 2(f), there are two peaks around the detunings $\Delta = \pm J$ in the strong-coupling regime. This phenomenon can be understood by analyzing the energy spectrum shown in Fig. 1(d): the transition process $|0,0\rangle_0 \rightarrow |1,1\rangle_{\pm}$ is resonantly enhanced with detunings $\Delta = \pm J$. As a consequence, we can shift the optimal value of the detuning for entanglement by tuning the coupling strength J as shown in Fig. 3(b).

Figure 4 shows the second-order correlation functions [$g_n^{(2)}(0)$ and $g_m^{(2)}(0)$] and cross-correlation function $g_{nm}^{(2)}(0)$ with the coupling strength J from weak to strong. The mean photon (phonon) number [$\langle n \rangle = \langle m \rangle$] and logarithmic negativity E_N increase with the enhancing of the coupling strength J . As shown in Fig. 4(b), the cross-correlation function $g_{nm}^{(2)}(0)$ decreases with the increasing of the mean photon (phonon) number [$\langle n \rangle = \langle m \rangle$], and the numerical results (red dashed curve) agrees well with the analytical results given in Eq. (15) (blue short-dashed curve). The second-order correlation functions [$g_n^{(2)}(0)$ and $g_m^{(2)}(0)$] increases first with the mean photon (phonon) number, and then decreases with the coupling strength J , as the excitations of states $|2,1\rangle_{\pm} \equiv (|g\rangle|2,1\rangle \pm |e\rangle|1,0\rangle)/\sqrt{2}$ and $|1,2\rangle_{\pm} \equiv (|g\rangle|1,2\rangle \pm |e\rangle|0,1\rangle)/\sqrt{2}$ are suppressed for the enhancement of the effective damping rates with the coupling strength J . The suitable coupling strength J for observing correlated single photons and single phonons, i.e., $g_n^{(2)}(0) = g_m^{(2)}(0) \ll 1$ and $g_{nm}^{(2)}(0) \gg 1$, is $J \ll \kappa$ or $J \gg \kappa$.

Generally, the damping rate of the mechanical mode is much smaller than the damping rate of the optical mode. However, the effective damping of the mechanical mode can be controlled and significantly enhanced by coupling the mechanical mode to an auxiliary op-

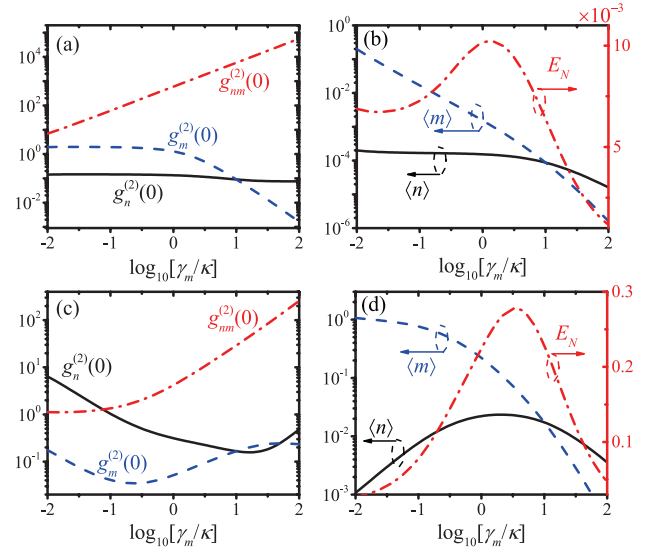


FIG. 5. (Color online) (a) and (c) the equal-time second-order correlation functions [$g_n^{(2)}(0)$ and $g_m^{(2)}(0)$] and cross-correlation function $g_{nm}^{(2)}(0)$ are plotted as functions of the mechanical damping rate $\log_{10}[\gamma_m/\kappa]$. (b) and (d), the mean photon (phonon) number [$\langle n \rangle$ and $\langle m \rangle$] and the logarithmic negativity E_N are plotted as functions of the mechanical damping rate $\log_{10}[\gamma_m/\kappa]$. We set $J = 0.1\kappa$ in (a) and (b) and set $J = 100\kappa$ in (c) and (d). Other used parameters are $|\Delta| = J$, $\gamma_c = 10\kappa$, $\Omega = \kappa$, and $m_{\text{th}} = 0$.

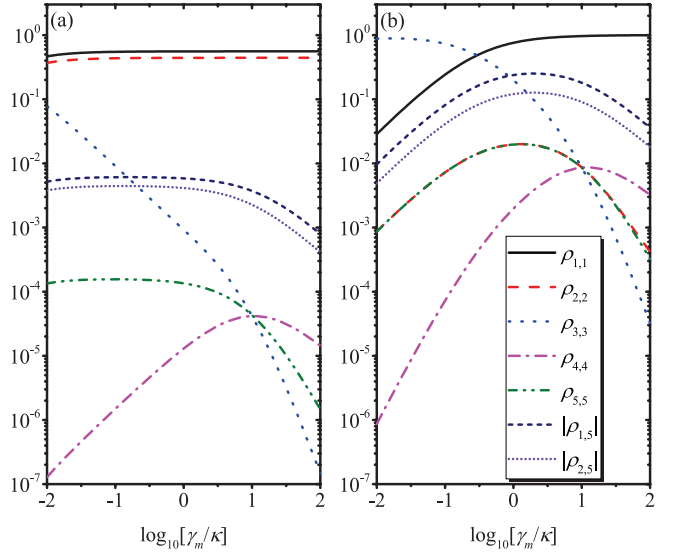


FIG. 6. (Color online) The elements of the density matrix ρ from Eq. (9) in the steady state are plotted as functions of the mechanical damping rate $\log_{10}[\gamma_m/\kappa]$, where $\rho_{1,1} = \langle g| \langle 0,0 | \rho | g \rangle | 0,0 \rangle$, $\rho_{2,2} = \langle e| \langle 0,0 | \rho | e \rangle | 0,0 \rangle$, $\rho_{3,3} = \langle g| \langle 0,1 | \rho | g \rangle | 0,1 \rangle$, $\rho_{4,4} = \langle g| \langle 1,0 | \rho | g \rangle | 1,0 \rangle$, $\rho_{5,5} = \langle g| \langle 1,1 | \rho | g \rangle | 1,1 \rangle$, $\rho_{1,5} = \langle g| \langle 0,0 | \rho | g \rangle | 1,1 \rangle$, $\rho_{2,5} = \langle e| \langle 0,0 | \rho | g \rangle | 1,1 \rangle$. We set $J = 0.1\kappa$ in (a) and set $J = 100\kappa$ in (b). Other used parameters are $|\Delta| = J$, $\gamma_c = 10\kappa$, $\Omega = \kappa$, and $m_{\text{th}} = 0$.

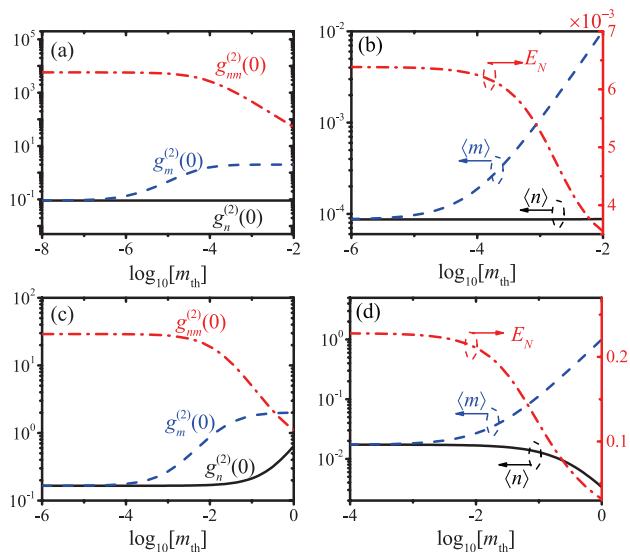


FIG. 7. (Color online) (a) and (c) the equal-time second-order correlation functions $[g_n^{(2)}(0)$ and $g_m^{(2)}(0)]$ and cross-correlation function $g_{nm}^{(2)}(0)$ are plotted as functions of the mean thermal phonon number $\log_{10}[m_{\text{th}}]$. (b) and (d), the mean photon (phonon) number $[\langle n \rangle]$ and the logarithmic negativity E_N are plotted as functions of the mean thermal phonon number $\log_{10}[m_{\text{th}}]$. We set $J = 0.1\kappa$ in (a) and (b) and set $J = 100\kappa$ in (c) and (d). Other used parameters are $|\Delta| = J$, $\gamma_c = \gamma_m = 10\kappa$, and $\Omega = \kappa$.

tical mode [60–63]. In addition, the phonon statistics can be observed indirectly by measuring statistics of the photons output from the auxiliary optical mode [64–67]. The dependence of the second-order correlation functions $[g_n^{(2)}(0)$ and $g_m^{(2)}(0)]$ and cross-correlation function $g_{nm}^{(2)}(0)$ on the mechanical damping rate γ_m is shown in Fig. 5. In the weak-coupling case [Figs. 5(a) and 5(b)], the correlation and cross-correlation functions change monotonically with the mechanical damping rate. In the strong-coupling case [Figs. 5(c) and 5(d)], the correlation and cross-correlation functions changing non-monotonously with the mechanical damping rate. The mean phonon number $\langle m \rangle$ decreases rapidly with the mechanical damping rate in both weak- and strong-coupling regimes and the mean photon number $\langle n \rangle$ decreases monotonously for weak coupling ($J \ll \kappa$). While $\langle n \rangle$ increases first and then decreases with the mechanical damping rate in the strong coupling regime ($J \gg \kappa$), i.e., we can enhance photon emission by increasing the mechanical damping rate when $\gamma_m < \kappa$. Moreover, there is a optimal mechanical damping rate γ_m for entanglement E_N around the point $\gamma_m \approx 1.32\kappa$ ($\gamma_m \approx 3.47\kappa$) in the case of $J = 0.1\kappa$ ($J = 100\kappa$).

These interesting phenomena can be understood by the probability distribution in the bare states as shown in Fig. 6, where $\rho_{1,1} = \langle g| \langle 0,0 | \rho | g \rangle | 0,0 \rangle$, $\rho_{2,2} = \langle e| \langle 0,0 | \rho | e \rangle | 0,0 \rangle$, $\rho_{3,3} = \langle g| \langle 0,1 | \rho | g \rangle | 0,1 \rangle$, $\rho_{4,4} = \langle g| \langle 1,0 | \rho | g \rangle | 1,0 \rangle$, $\rho_{5,5} = \langle g| \langle 1,1 | \rho | g \rangle | 1,1 \rangle$, $\rho_{1,5} =$

$\langle g| \langle 0,0 | \rho | g \rangle | 1,1 \rangle$, $\rho_{2,5} = \langle e| \langle 0,0 | \rho | g \rangle | 1,1 \rangle$. It is clear that we have $\rho_{3,3} \approx \rho_{4,4} \approx \rho_{5,5}$ around $\gamma_m = \gamma_c$, which is agree with Eqs. (13) and (14). In the weak-coupling regime ($J \ll \kappa$) as shown in Fig. 6(a), most of the probability is distributed in the states $|g\rangle|0,0\rangle$ and $|e\rangle|0,0\rangle$; the probability in states $|g\rangle|1,1\rangle$ (as well as the off-diagonal elements $|\rho_{1,4}|$ and $|\rho_{1,5}|$, which determine the entanglement E_N between the photons and phonons) increases slowly in the regime of $\gamma_m < \kappa$, and decreases rapidly when $\gamma_m > \kappa$; the probability in single phonon state $|g\rangle|0,1\rangle$ (single photon state $|g\rangle|1,0\rangle$) decreases (increases) in the regime of $\gamma_m < \gamma_c$, and decreases rapidly when $\gamma_m > \gamma_c$. Differently, in the strong-coupling regime ($J \gg \kappa$) as shown in Fig. 6(b), most of the probability (87.5%) is distributed in the single phonon state $|g\rangle|0,1\rangle$ when $\gamma_m \ll \kappa$, as the damping rate of the state $|g\rangle|0,1\rangle$ is much smaller than the other states; the probability in the ground state $|g\rangle|0,0\rangle$ increase monotonously with the mechanical damping rate; the probability in states $|e\rangle|0,0\rangle$ and $|g\rangle|1,1\rangle$ are almost the same, i.e., $\rho_{2,2} \approx \rho_{5,5}$, and they (as well as the off-diagonal elements $|\rho_{1,4}|$ and $|\rho_{1,5}|$) increases first and then decreases with the mechanical damping rate, which is corresponding to the phenomena of photon emission and entanglement enhancing by increasing the mechanical damping rate when $\gamma_m < \kappa$.

The thermal effect of the mechanical mode on the statistic properties of the generated photons and phonons are shown in Fig. 7. It is clear that the thermal phonons have a significant effect on the statistic properties of the generated photons and phonons. As the mean phonon number is much larger in the strong-coupling regime than the one in the weak-coupling regime, the correlated and entangled photon blockade and phonon blockade in the strong-coupling regime is more robust against the thermal noise than the one in the weak-coupling regime.

IV. CONCLUSIONS

In summary, we have studied the photon and phonon statistics, and the quantum correlation between photons and phonons in a hybrid optomechanical system including an atom-photon-phonon (tripartite) interaction. We have shown that both the photon and phonon blockade can be observed in the same parameter area, and the generated single photons and single phonons are correlated and entangled with each other. Moreover, the single entangled photon-phonon pairs can be observed in both the weak and strong tripartite interaction regime. The phonons with low-loss can be used for quantum memories, and photons are suitable for the transmission of quantum information. The generated single entangled photon-phonon pairs will have applications in quantum communication and the hybrid optomechanical system can serve as quantum transducers in building hybrid quantum networks. In addition, the basic mechanism of this work can be generalized to a nondegenerate two-photon Jaynes-Cummings model [68, 69], to generate entangled photon pairs with different frequency, such as entangled microwave-optical photon pairs [70].

Acknowledgement

We thank Yan-Jun Zhao, Hui Wang, and Qiang Zheng for helpful discussions. X.-W.X. was supported by the National Natural Science Foundation of China (NSFC) under Grant No. 11604096. A.-X.C. is supported by

NSFC under Grant No. 11775190. J.-Q.L. is supported in part by National Natural Science Foundation of China under Grants No. 11822501 and No. 11774087, and Natural Science Foundation of Hunan Province, China under Grant No. 2017JJ1021.

-
- [1] M. Aspelmeyer, T. J. Kippenberg, and F. Marquardt, Cavity Optomechanics, *Rev. Mod. Phys.* **86**, 1391 (2014).
- [2] A. Imamoglu, H. Schmidt, G. Woods, and M. Deutsch, Strongly Interacting Photons in a Nonlinear Cavity, *Phys. Rev. Lett.* **79**, 1467 (1997).
- [3] K. M. Birnbaum, A. Boca, R. Miller, A. D. Boozer, T. E. Northup, and H. J. Kimble, Photon blockade in an optical cavity with one trapped atom, *Nature (London)* **436**, 87 (2005).
- [4] Y. X. Liu, A. Miranowicz, Y. B. Gao, J. Bajer, C. P. Sun, and F. Nori, Qubit-induced phonon blockade as a signature of quantum behavior in nanomechanical resonators, *Phys. Rev. A* **82**, 032101 (2010).
- [5] P. Rabl, Photon Blockade Effect in Optomechanical Systems, *Phys. Rev. Lett.* **107**, 063601 (2011).
- [6] A. Nunnenkamp, K. Børkje, and S. M. Girvin, Single-Photon Optomechanics, *Phys. Rev. Lett.* **107**, 063602 (2011).
- [7] K. Stannigel, P. Komar, S. J. M. Habraken, S. D. Bennett, M. D. Lukin, P. Zoller, and P. Rabl, Optomechanical Quantum Information Processing with Photons and Phonons, *Phys. Rev. Lett.* **109**, 013603 (2012).
- [8] A. Kronwald, M. Ludwig, and F. Marquardt, Full photon statistics of a light beam transmitted through an optomechanical system, *Phys. Rev. A* **87**, 013847 (2013).
- [9] X. W. Xu, Y. J. Li, and Y. X. Liu, Photon-induced tunneling in optomechanical systems, *Phys. Rev. A* **87**, 025803 (2013).
- [10] J. Q. Liao and F. Nori, Photon blockade in quadratically coupled optomechanical systems, *Phys. Rev. A* **88**, 023853 (2013).
- [11] X. Y. Lü, Y. Wu, J. R. Johansson, H. Jing, J. Zhang, and F. Nori, Squeezed Optomechanics with Phase-Matched Amplification and Dissipation, *Phys. Rev. Lett.* **114**, 093602 (2015).
- [12] D. Hu, S. Y. Huang, J. Q. Liao, L. Tian, and H. S. Goan, Quantum coherence in ultrastrong optomechanics, *Phys. Rev. A* **91**, 013812 (2015).
- [13] H. Xie, G. W. Lin, X. Chen, Z. H. Chen, and X. M. Lin, Single-photon nonlinearities in a strongly driven optomechanical system with quadratic coupling, *Phys. Rev. A* **93**, 063860 (2016).
- [14] H. Seok and E. M. Wright, Antibunching in an optomechanical oscillator, *Phys. Rev. A* **95**, 053844 (2017).
- [15] H. Xie, C. G. Liao, X. Shang, M. Y. Ye, and X. M. Lin, Phonon blockade in a quadratically coupled optomechanical system, *Phys. Rev. A* **96**, 013861 (2017).
- [16] X. W. Xu and Y. J. Li, Antibunching photons in a cavity coupled to an optomechanical system, *J. Phys. B* **46**, 035502 (2013).
- [17] V. Savona, Unconventional photon blockade in coupled optomechanical systems, arXiv:1302.5937.
- [18] H. Q. Shi, X. T. Zhou, X. W. Xu, and N. H. Liu, Tunable phonon blockade in quadratically coupled optomechanical systems. *Sci. Rep.* **8**, 2212 (2018).
- [19] M. Wang, X. Y. Lü, A. Miranowicz, T. S. Yin, Y. Wu, and F. Nori, Unconventional phonon blockade via atom-photon-phonon interaction in hybrid optomechanical systems, arXiv:1806.03754 [quant-ph].
- [20] B. Li, R. Huang, X. W. Xu, A. Miranowicz, and H. Jing, Nonreciprocal unconventional photon blockade in a spinning optomechanical system, arXiv:1901.10784 [quant-ph].
- [21] R. Riedinger, S. Hong, R. A. Norte, J. A. Slater, J. Shang, A. G. Krause, V. Anant, M. Aspelmeyer, and S. Gröblacher, Non-classical correlations between single photons and phonons from a mechanical oscillator, *Nature* **530**, 313 (2016).
- [22] X. W. Xu, H. Q. Shi, A. X. Chen, and Y. X. Liu, Cross-correlation between photons and phonons in quadratically coupled optomechanical systems, *Phys. Rev. A* **98**, 013821 (2018).
- [23] D. Vitali, S. Gigan, A. Ferreira, H. R. Böhm, P. Tombesi, A. Guerreiro, V. Vedral, A. Zeilinger, and M. Aspelmeyer, Optomechanical Entanglement between a Movable Mirror and a Cavity Field, *Phys. Rev. Lett.* **98**, 030405 (2007).
- [24] M. J. Hartmann and M. B. Plenio, Steady State Entanglement in the Mechanical Vibrations of Two Dielectric Membranes, *Phys. Rev. Lett.* **101**, 200503 (2008).
- [25] K. Børkje, A. Nunnenkamp, and S. M. Girvin, Proposal for Entangling Remote Micromechanical Oscillators via Optical Measurements, *Phys. Rev. Lett.* **107**, 123601 (2011).
- [26] Sh. Barzanjeh, M. Abdi, G. J. Milburn, P. Tombesi, and D. Vitali, Reversible Optical-to-Microwave Quantum Interface, *Phys. Rev. Lett.* **109**, 130503 (2012).
- [27] Y. D. Wang and A. A. Clerk, Using Interference for High Fidelity Quantum State Transfer in Optomechanics, *Phys. Rev. Lett.* **108**, 153603 (2012).
- [28] L. Tian, Adiabatic State Conversion and Pulse Transmission in Optomechanical Systems, *Phys. Rev. Lett.* **108**, 153604 (2012).
- [29] T. A. Palomaki, J. D. Teufel, R. W. Simmonds, and K. W. Lehnert, Entangling Mechanical Motion with Microwave Fields, *Science* **342**, 710 (2013).
- [30] R. Riedinger, A. Wallucks, I. Marinković, C. Löschnauer, M. Aspelmeyer, S. Hong, and S. Gröblacher, Remote quantum entanglement between two micromechanical oscillators, *Nature* **556**, 473 (2018).
- [31] C. F. Ockeloen-Korppi, E. Damskägg, J.-M. Pirkkalainen, M. Asjad, A. A. Clerk, F. Massel, M. J. Woolley, and M. A. Sillanpää, Stabilized entanglement of massive mechanical oscillators, *Nature* **556**, 478 (2018).
- [32] I. Marinković, A. Wallucks, R. Riedinger, S. Hong, M. Aspelmeyer, and S. Gröblacher, Optomechanical Bell Test, *Phys. Rev. Lett.* **121**, 220404 (2018).

- [33] W. J. Nie, Y. H. Lan, Y. Li, and S. Y. Zhu, Effect of the Casimir force on the entanglement between a levitated nanosphere and cavity modes, *Phys. Rev. A* **86**, 063809 (2012).
- [34] X. W. Xu, Y. J. Zhao, and Y. X. Liu, Entangled-state engineering of vibrational modes in a multimembrane optomechanical system, *Phys. Rev. A* **88**, 022325 (2013).
- [35] J. Q. Liao, Q. Q. Wu, and F. Nori, Entangling two macroscopic mechanical mirrors in a two-cavity optomechanical system, *Phys. Rev. A* **89**, 014302 (2014).
- [36] X. Y. Lü, G. L. Zhu, L. L. Zheng, and Y. Wu, Entanglement and quantum superposition induced by a single photon, *Phys. Rev. A* **97**, 033807 (2018).
- [37] M. Paternostro, D. Vitali, S. Gigan, M. S. Kim, C. Brukner, J. Eisert, and M. Aspelmeyer, Creating and Probing Multipartite Macroscopic Entanglement with Light, *Phys. Rev. Lett.* **99**, 250401 (2007).
- [38] C. Genes, A. Mari, P. Tombesi, and D. Vitali, Robust entanglement of a micromechanical resonator with output optical fields, *Phys. Rev. A* **78**, 032316 (2008).
- [39] H. T. Tan and G. X. Li, Multicolor quadripartite entanglement from an optomechanical cavity, *Phys. Rev. A* **84**, 024301 (2011).
- [40] A. Xuereb, M. Barbieri, and M. Paternostro, Multipartite optomechanical entanglement from competing nonlinearities, *Phys. Rev. A* **86**, 013809 (2012).
- [41] J. Li, S. Y. Zhu, and G. S. Agarwal, Magnon-Photon-Phonon Entanglement in Cavity Magnomechanics, *Phys. Rev. Lett.* **121**, 203601 (2018).
- [42] F. Tian, H. Sumikura, E. Kuramochi, M. Takiguchi, M. Ono, A. Shinya, and M. Notomi, All-optical dynamic modulation of spontaneous emission rate in hybrid optomechanical cavity quantum electrodynamics systems, arXiv:1901.07691 [physics.optics].
- [43] Y. Chang, H. Ian, and C. P. Sun, Triple coupling and parameter resonance in quantum optomechanics with a single atom, *J. Phys. B: At. Mol. Opt. Phys.* **42**, 215502 (2009).
- [44] M. Cotrufo, A. Fiore, and E. Verhagen, Coherent Atom-Phonon Interaction through Mode Field Coupling in Hybrid Optomechanical Systems, *Phys. Rev. Lett.* **118**, 133603 (2017).
- [45] J. D. Teufel, D. Li, M. S. Allman, K. Cicak, A. J. Sirois, J. D. Whittaker, and R. W. Simmonds, Circuit cavity electromechanics in the strong-coupling regime, *Nature (London)* **471**, 204 (2011).
- [46] F. Massel, S. Un Cho, J.-M. Pirkkalainen, P. J. Hakonen, T. T. Heikkilä, and M. A. Sillanpää, Multimode circuit optomechanics near the quantum limit, *Nat. Commun.* **3**, 987 (2012).
- [47] J. Suh, A. J. Weinstein, C. U. Lei, E. E. Wollman, S. K. Steinke, P. Meystre, A. A. Clerk, and K. C. Schwab, Mechanically detecting and avoiding the quantum fluctuations of a microwave field, *Science* **344**, 1262 (2014).
- [48] J. D. Thompson, B. M. Zwickl, A. M. Jayich, F. Marquardt, S. M. Girvin, and J. G. E. Harris, Strong dispersive coupling of a high-finesse cavity to a micromechanical membrane, *Nature (London)* **452**, 72 (2008).
- [49] N. E. Flowers-Jacobs, S.W. Hoch, J. C. Sankey, A. Kashkanova, A. M. Jayich, C. Deutsch, J. Reichel, and J. G. E. Harris, Fiber-Cavity-Based Optomechanical Device, *Appl. Phys. Lett.* **101**, 221109 (2012).
- [50] H. Xu, D. Mason, L. Jiang, and J. G. E. Harris, Topological energy transfer in an optomechanical system with exceptional points, *Nature (London)* **537**, 80 (2016).
- [51] H. Xu, U. Kemiktarak, J. Fan, S. Ragole, J. Lawall, and J. M. Taylor, Observation of optomechanical buckling transitions, *Nat. Commun.* **8**, 14481 (2017).
- [52] H. J. Carmichael, *An Open Systems Approach to Quantum Optics*, Lecture Notes in Physics Vol. 18 (Springer-Verlag, Berlin, 1993).
- [53] G. Vidal and R. F. Werner, Computable measure of entanglement, *Phys. Rev. A* **65**, 032314 (2002).
- [54] S. E. Harris, Electromagnetically Induced Transparency, *Phys. Today* **50**(7), 36 (1997).
- [55] M. Fleischhauer, A. Imamoglu, and J. P. Marangos, Electromagnetically induced transparency: Optics in coherent media, *Rev. Mod. Phys.* **77**, 633 (2005).
- [56] G. S. Agarwal and S. Huang, Electromagnetically induced transparency in mechanical effects of light, *Phys. Rev. A* **81**, 041803(R) (2010).
- [57] S. Weis, R. Riviere, S. Deleglise, E. Gavartin, O. Arcizet, A. Schliesser, and T. J. Kippenberg, Optomechanically Induced Transparency, *Science* **330**, 1520 (2010).
- [58] A. H. Safavi-Naeini, T. P. Mayer Alegre, J. Chan, M. Eichenfield, M. Winger, Q. Lin, J. T. Hill, D. E. Chang, and O. Painter, Electromagnetically induced transparency and slow light with optomechanics, *Nature (London)* **472**, 69 (2011).
- [59] G. Adesso, A. Serafini, and F. Illuminati, Extremal entanglement and mixedness in continuous variable systems, *Phys. Rev. A* **70**, 022318 (2004).
- [60] I. Wilson-Rae, N. Nooshi, W. Zwerger, and T. J. Kippenberg, Theory of Ground State Cooling of a Mechanical Oscillator Using Dynamical Backaction, *Phys. Rev. Lett.* **99**, 093901 (2007).
- [61] F. Marquardt, J. P. Chen, A. A. Clerk, and S. M. Girvin, Quantum Theory of Cavity-Assisted Sideband Cooling of Mechanical Motion, *Phys. Rev. Lett.* **99**, 093902 (2007).
- [62] Y. Li, Y. D. Wang, F. Xue, and C. Bruder, Quantum theory of transmission line resonator-assisted cooling of a micromechanical resonator, *Phys. Rev. B* **78**, 134301 (2008).
- [63] X. W. Xu, Y. X. Liu, C. P. Sun, and Y. Li, Mechanical \mathcal{PT} symmetry in coupled optomechanical systems, *Phys. Rev. A* **92**, 013852 (2015).
- [64] N. Didier, S. Pugnetti, Y. M. Blanter, and R. Fazio, Detecting phonon blockade with photons, *Phys. Rev. B* **84**, 054503 (2011).
- [65] T. Ramos, V. Sudhir, K. Stannigel, P. Zoller, and T. J. Kippenberg, Nonlinear Quantum Optomechanics via Individual Intrinsic Two-Level Defects, *Phys. Rev. Lett.* **110**, 193602 (2013).
- [66] J. D. Cohen, S. M. Meenehan, G. S. MacCabe, S. Groblacher, A. H. Safavi-Naeini, F. Marsili, M. D. Shaw, and O. Painter, Phonon counting and intensity interferometry of a nanomechanical resonator, *Nature (London)* **520**, 522 (2015).
- [67] X. W. Xu, A. X. Chen, and Y. X. Liu, Phonon blockade in a nanomechanical resonator resonantly coupled to a qubit, *Phys. Rev. A* **94**, 063853 (2016).
- [68] S. C. Gou, Quantum behavior of a two-level atom interacting with two modes of light in a cavity, *Phys. Rev. A* **40**, 5116 (1989).
- [69] M. M. Ashraf and M. S. K. Razmi, Atomic-dipole squeezing and emission spectra of the nondegenerate two-photon Jaynes-Cummings model, *Phys. Rev. A* **45**, 8121 (1992).

- [70] C. Zhong, Z. Wang, C. Zou, M. Zhang, X. Han, W. Fu, M. Xu, S. Shankar, M. H. Devoret, H. X. Tang, and L. Jiang, Heralded Generation and Detection of Entangled Microwave–Optical Photon Pairs, arXiv:1901.08228 [quant-ph].